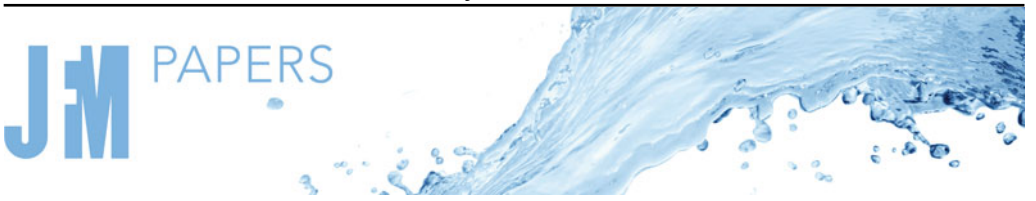
J. Fluid Mech. (2026), *vol.* 1037, A49, doi:10.1017/jfm.2026.11689



Generating wall-bounded turbulent inflows at high Reynolds numbers

Ronith Stanly[1], Timofey Mukha[2], Martin Karp[1], Stefano Markidis[3] and Philipp Schlatter[1,4]

[1]Department of Engineering Mechanics, KTH Royal Institute of Technology, Stockholm SE-100 44, Sweden

[2]Computer, Electrical and Mathematical Sciences and Engineering Division, King Abdullah University of Science and Technology (KAUST), Thuwal 23955-6900, Kingdom of Saudi Arabia

[3]Division of Computational Science and Technology, EECS, KTH Royal Institute of Technology, Stockholm SE-100 44, Sweden

[4]Institute of Fluid Mechanics (LSTM), Friedrich–Alexander–Universität Erlangen–Nürnberg (FAU), Erlangen DE-910 58, Germany

Corresponding authors: Timofey Mukha, timofey.mukha@kaust.edu.sa; Ronith Stanly, ronith@kth.se

(Received 22 October 2025 UTC; revised 15 March 2026 UTC; accepted 7 May 2026 UTC)

One of the main challenges in simulating high Reynolds number (Re) turbulent boundary layers (TBLs) is the long streamwise distance required for large-scale outer-layer structures to develop, making such simulations prohibitively expensive. We propose an inflow generation method for high Re wall turbulence that leverages the known structure and scaling laws of TBLs. Pre-multiplied spectra of streamwise velocity show that with an increase in Re the outer region grows and occupies more of the spanwise wavenumber space in proportion to the increase in Re, while the inner region remains approximately the same. Exploiting this behaviour, we generate inflow conditions for a target Re by starting from cross-stream velocity slices at a lower base Re. In spectral space, we identify the inner- and outer-region wavenumbers, and shift the outer-region components proportionally to the desired Re increase. We examine the capability of this method by scaling velocity slices at $Re_\theta = 2240$ and 4430 to $Re_\theta = 8000$, and using them as inflow conditions for direct numerical simulations of TBLs growing in the range $Re_\theta = 8000 - 9000$, with Re_θ being the Reynolds number based on the momentum-loss thickness θ. The predicted skin friction coefficient and shape factor, regardless of the base Re_θ tested, lie within $\pm 3.5\,\%$ and $\pm 0.5\,\%$, respectively, of that of a precursor simulation right from the inlet. Reynolds stresses match very well after approximately $8\,\delta_{99_0}$. The development length in terms of the Reynolds stresses is approximately $8\delta_{99_0}$, where δ_{99_0} is the boundary

© The Author(s), 2026. Published by Cambridge University Press. This is an Open Access article, distributed under the terms of the Creative Commons Attribution licence (https://creativecommons.org/licenses/by/4.0/), which permits unrestricted re-use, distribution and reproduction, provided the original article is properly cited.

https://doi.org/10.1017/jfm.2026.11689 Published online by Cambridge University Press

layer thickness at the inlet. This gives an order of magnitude reduction in development length compared with other methods proposed in the literature.

Key words: turbulent boundary layers, turbulence simulation

1. Introduction

Improving our fundamental understanding of high Reynolds number (*Re*) turbulent boundary layers requires advancements in both experimental methods as well as simulation techniques. This would, for instance, enable us to answer questions such as the extent of applicability of Taylor's hypothesis by knowing the scale-dependent distribution of convection velocities, to unravel the influence of large-scale structures on near-wall turbulence or to find out the differences between canonical cases of wall turbulence, *viz.*, pipes (Massaro *et al.* 2024*b*), channels (Monty *et al.* 2007, 2009) and turbulent boundary layers (Hutchins & Marusic 2007; Smits, McKeon & Marusic 2011).

The focus of this current work is on simulation methods for spatially developing turbulent boundary layers, where the turbulence inflow condition is often a limiting factor. We note that an alternative approach is to consider a so-called temporally developing boundary layer (Spalart 1988; Biau 2023; Wynn *et al.* 2025), which is streamwise periodic. However, spatially developing layers are naturally occurring phenomena crucial to many industrial applications. This justifies the need to further develop a simulation methodology for their study.

A good turbulent inflow method is expected to develop the flow to the required turbulent state in as short a streamwise distance as possible (Tabor & Baba-Ahmadi 2010). This becomes difficult at higher *Re*, because the large structures in the outer region take longer to develop (Sillero, Jiménez & Moser 2013). Wu (2017) and Dhamankar, Blaisdell & Lyrintzis (2018) provide a concise overview of several methods that can be used to provide an inflow condition. In principle, we can distinguish two basic types: (i) methods that re-use real turbulent fields after some transformation and (ii) methods that create artificial turbulence, and mixtures of the two. Generally, artificially generating turbulence incurs little computational overhead, but leads to a larger development length. On the other hand, precursor-based methods provide high-quality inflow, but require an additional simulation, the cost of which grows with *Re*. Having means to reduce this cost would therefore be extremely beneficial. In this work, we propose a novel way to do that.

Central to our approach is the idea to utilise the known structure of the coherent eddies (Robinson 1991) within a turbulent boundary layer to derive the inflow generation procedure. The underlying theory stems from the works of Perry & Chong (1982), Perry & Marušić (1995) and Marušić & Perry (1995), who demonstrated, using the attached eddy hypothesis of Townsend (1956, 1976), that the first- and second-order statistics of a turbulent boundary layer can be reproduced using a superposition of these coherent structures. A short overview of previous works that tried to leverage this follows.

Subbareddy *et al.* (2006) proposed an inflow condition where they assumed the flow was populated by hairpin vortices with a given population density. The Biot–Savart law was used to compute the velocity field these vortices induced around them and image vortices at the wall were used to enforce the no-penetration condition. However, they mentioned that it 'would be impractical to resolve' the inner-scale structures 'at moderate to high Reynolds number' flows using this idea 'on small/medium sized grids' and that the method was better suited for large-eddy simulation (LES) or hybrid Reynolds-Averaged Navier–Stokes-LES which did not resolve the wall. Sandham, Yao & Lawal (2003)

https://doi.org/10.1017/jfm.2026.11689 Published online by Cambridge University Press

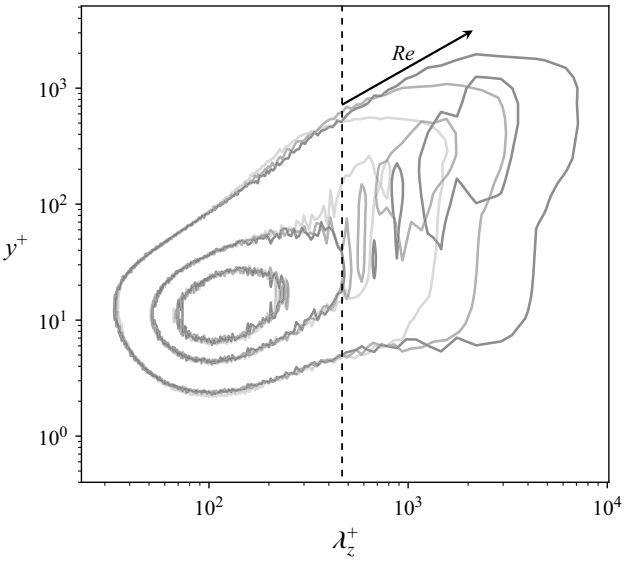


Figure 1. Pre-multiplied spectra of streamwise velocity u at increasing Re ($Re_\theta = 2240$, 4430, 8000; contour lines of increasing darkness show increasing Re), i.e. $E_{uu}(k_z) \cdot k_z/u_\tau^2$. Here, y is the wall-normal coordinate. Notice that the inner region (left of the vertical dashed line) remains the same size, whereas the outer region (right of the vertical dashed line) grows with increasing Re. For each level of darkness, contour lines are plotted for levels [0.5, 1.5, 2.5, 4.0]. Data from Eitel-Amor, Örlü & Schlatter (2014).

proposed a simple coherent structure-based model which split the boundary layer into two regions: an inner region populated with lifted streaks and an outer region populated with three-dimensional eddies. Their deterministic model introduced disturbances corresponding to the inner and outer regions along with their associated phase information. Touber & Sandham (2009) later evaluated this method and found that it generated a mean velocity profile with an unrealistic outer region, and resulted in a spurious secondary peak in turbulence intensity and Reynolds shear-stress profiles in the outer region. These could be corrected by running several precursors and tuning certain parameters as in Sandberg & Sandham (2008) and Sandham & Sandberg (2009). In another work, Pamiès *et al.* (2009) proposed a modification to the synthetic eddy method by Jarrin *et al.* (2006) for LES of spatially developing boundary layers. They split the random structures into those belonging to different modes and included their proper length, time, velocity and vorticity contents, to better represent the vortex structures inside a turbulent boundary layer in the wall-normal direction. With this they were able to better specify the information of the modes for the buffer and logarithmic layers which helped reduce their development length.

While the above studies focused on artificial turbulence, we seek to leverage the same theory but in the context of precursor-based inflow generation. In particular, the proposed method relies on the observed energy scaling of coherent structures in spectral space. The inner-scaled spectra of streamwise velocity pre-multiplied with spanwise wavenumbers (figure 1) show that with an increase in Re the outer region grows and occupies more spanwise wavenumbers as opposed to the inner region that remains nearly unchanged. It follows that given cross-stream velocity slices at a given Re, a higher-Re inflow could be produced by a rescaling of the outer-layer structures in the original data.

Using the proposed method, time-dependent cross-stream velocity slices of a turbulent boundary layer at a given Re are first split into inner and outer regions in spectral space, followed by scaling (in space, time and energy) of the spanwise wavenumbers

https://doi.org/10.1017/jfm.2026.11689 Published online by Cambridge University Press

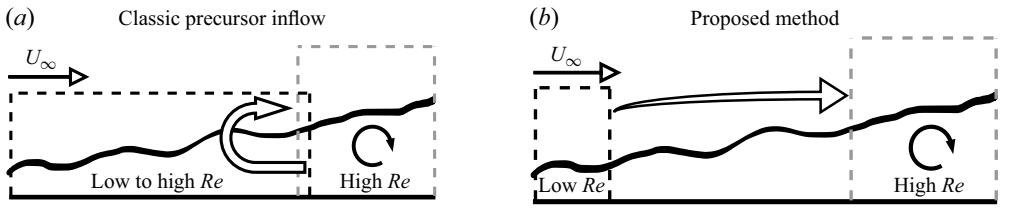


Figure 2. Schematic of the proposed method highlighting its potential to reduce computational cost by up-scaling low-*Re* precursor data to high *Re*. (*a*) In classic precursor or existing methods, the precursor domain must grow with the target *Re*. (*b*) The proposed scaling method enables a small, fixed-size precursor domain regardless of target *Re*. Black dashed boxes show precursor domains; grey dashed boxes show main turbulent boundary layer (TBL) simulation domains. Single-lined arrows indicate flow direction, double-lined arrows indicate Dirichlet inflow application.

corresponding to the outer region appropriately to then reconstruct velocity fields at any higher *Re* of interest. As schematically shown in figure 2, such a procedure enables a leap from low *Re* precursor data to much higher *Re*. This avoids the need for prohibitively expensive precursor domains, which must be larger the higher the target *Re* one aims to simulate.

In the remainder of this paper, we first describe the scaling method in detail in § 2, followed by demonstrating its application as inflow condition in § 3. Final conclusions and outlook are given in § 4.

2. Methodology

Necessary notation is now introduced before proceeding with a detailed description of the proposed inflow generation method. The superscript tg will be used to denote quantities at the target Reynolds number, Re^{tg}, at which the inflow is to be generated. Similarly, the superscript bs will denote quantities already available at some base Reynolds number, $Re^{bs} < Re^{tg}$. Further, u_i will refer to the Cartesian projections of the velocity field, where $i \in \{1, 2, 3\}$ denotes the coordinate index. The values of i correspond to the streamwise, wall-normal and spanwise directions. The triples (x, y, z) and (u, v, w) will also be used for the coordinates and velocity components, respectively. Similarly, U_i will denote the mean value of u_i, and a prime will be used for fluctuations, i.e. $u_i = U_i + u_i'$. The root-mean-square values of the fluctuations will be referred to as u_{rms}, v_{rms} and w_{rms}. The $+$ superscript will be used to denote scaling with inner-layer quantities, that is, the friction velocity u_τ and inner length scale l^*. The velocity of the free stream will be referred to as U_∞. Finally, the boundary layer thickness will be quantified in terms of momentum-loss thickness, θ, and the wall-normal location where $U_1 = 0.99U_\infty$, i.e. δ_{99}. The corresponding Reynolds numbers are Re_θ and $Re_{\delta_{99}}$. Additional notation will be introduced as necessary.

The Matlab implementation of the proposed method is available at https://github.com/ronithstanly/scaling_inflow and the time series data of velocity slices at Re^{bs}, from Eitel-Amor *et al.* (2014), used in this work can be made available upon request.

To obtain velocity fields at Re^{tg}, the proposed method requires the following two inputs:

(i) Time-dependent cross-stream velocity slices at a lower Re^{bs}.
(ii) The target Re^{tg}.

And, if the flow is not a generic zero-pressure-gradient TBL, appropriate scaling behaviour of the velocity spectral density and velocity profiles.

https://doi.org/10.1017/jfm.2026.11689 Published online by Cambridge University Press

Using the value of Re^{tg}, the following derived inputs are calculated: mean velocity profiles $U_i^{tg}(y)$ and the scaling factors for the outer-layer structures in space and time ($S_{\delta_{99}}$), and energy (S_E).

The velocity fields at Re^{bs} can be obtained by running a low-cost precursor, or simply taken from an existing database. The slices should be wide enough in z to incorporate the wider structures that would appear after applying the rescaling procedure. Otherwise, the enforced spanwise periodicity will introduce artificial correlations into the flow. Potential alternatives to avoid a very wide domain in the precursor are discussed in § 4.

An additional requirement is that, at Re^{bs}, the flow should have some large-scale structures present beyond an inner-scaled spanwise wavelength of $\lambda_z^+ > 500$, as seen in pre-multiplied spectra of streamwise velocity (figure 1). In other words, Re^{bs} should be high enough for outer scaling to be valid.

In this work, we use the database of Eitel-Amor *et al.* (2014), where a finely resolved LES was performed up to $Re_\theta = 8300$. Time series of cross-stream velocity slices sampled on a coarser y-grid (of 47 points) are available at $Re_\theta = 2240$, 3740, 4430, 5740 and 8000.

As will be shown below, $Re_\theta^{bs} = 2240$ is sufficiently high for the proposed method to work seamlessly (i.e. being able to scale velocity slices from Re_θ^{bs} to Re_θ^{tg} without knowing the shape of the spectra at Re_θ^{tg}). On the other hand, the extreme case of using a very low $Re_\theta^{bs} = 790$ requires hand tuning of the scaling parameters for space and energy by examining an existing database of pre-multiplied spectra of u at Re^{tg}. This is because the outer scaling does not hold true at such a low Re where viscous effects and interactions between the inner and outer regions are strong.

The mean streamwise velocity profile at any Re^{tg} can be obtained by using, for instance, the log law (Von Kármán 1930), Coles' law (Coles 1956), the composite profile (Monkewitz, Chauhan & Nagib 2007) or any other suitable universal profile (Subrahmanyam, Cantwell & Alonso 2022). For the mean wall-normal velocity profile, methods like the ones proposed by Wei, Li & Wang (2023) can be used. Alternatively, the continuity equation along with self-similarity can be employed to derive approximations. For the numerical experiments performed in this work, the database contained the information at Re^{tg}, so the mean velocity profiles are taken from there.

2.1. *Extracting inner and outer structures*

A discrete Fourier transform (DFT) is used to extract structures corresponding to the inner and outer regions from the velocity slices at Re^{bs}. The transform is applied along z in lieu of periodicity of the flow in that direction. The transform is defined as

$$\hat{u}_i^{(k_z)}(y,t) = \frac{1}{\sqrt{n_z}} \sum_{j=0}^{n_z-1} u_i\big(y, z_j, t\big) e^{-2\pi i k_z j/n_z}. \tag{2.1}$$

The normalisation using $\sqrt{n_z}$ ensures that the Parseval relation holds (Trefethen 2000; Bounchaleun 2019). Here, the wavenumber index k_z is related to the physical wavenumber k_z^{phys} as

$$k_z^{phys} = \frac{2\pi k_z}{L_z}, \tag{2.2}$$

where L_z is the size of the domain in z.

https://doi.org/10.1017/jfm.2026.11689 Published online by Cambridge University Press

Because the velocity field is real valued, we exploit the Hermitian symmetry of the DFT and retain only one half of the wavenumbers

$$k_z \in \left[0, 1, 2, \ldots, \frac{n_z}{2}\right]. \tag{2.3}$$

This modifies the normalisation factor in (2.1) to $\sqrt{n_z/2}$.

Following this, spanwise wavenumbers corresponding to the inner and outer regions of the TBL are extracted depending on their corresponding value of $\lambda_z{}^+$ which is calculated as

$$\lambda_z{}^+ = \frac{2\pi}{k_z l^*}, \tag{2.4}$$

obtained as $l^* = \nu/u_\tau$. Here, u_τ is the friction velocity calculated using wall-shear stress τ_w and density ρ, as $u_\tau = \sqrt{\tau_w/\rho}$. Following this, a range of k_z values corresponding approximately to $30 \leqslant \lambda_z{}^+ \leqslant 500$ is extracted to obtain the inner region (i.e. k_z^{inner}). For the outer region, the relevant range of k_z (i.e. k_z^{outer}) depends on Re^{bs} (see figure 1). For instance, for $Re_\theta = 2240$, k_z^{outer} is approximately $500 < \lambda_z{}^+ \leqslant 1700$, and for $Re_\theta = 4430$ it shifts to $750 < \lambda_z{}^+ \leq 3000$.

The $\hat{u_i}^{(k_z)}(y, t)$ for the selected wavenumbers are stacked into adjacent columns to construct the complex snapshot matrix. Singular value decomposition (SVD) is then performed in the wall-normal direction for each of those wavenumbers. This results in time coefficients, $a^{(k_z,n)}(t)$ of the nth proper orthogonal decomposition (POD) mode, and complex POD modes, $\hat{\varphi_i}^{(k_z,n)}(y)$. The above operations result in an expansion as follows:

$$\hat{u_i}^{(k_z)}(y, t) \approx \sum_{n=0}^{n_{modes}-1} a^{(k_z,n)}(t)\hat{\varphi_i}^{(k_z,n)}(y). \tag{2.5}$$

The time coefficients are used to scale the temporal evolution of those selected structures, as shown below. The SVD enables two extra possibilities: (i) to create a low-order model for the wall-normal dynamics, and (ii) to incorporate synthetically extended time coefficients generated by vector autoregression as described by Stanly *et al.* (2024). The latter provides a way to extend the time duration of the generated inflow beyond that of the precursor database. However, in principle, the SVD can be omitted and the rescaling performed directly on the Fourier coefficients.

2.2. *Scaling procedure*

Overall, scaling the velocity fields in Re involves shifting the spanwise wavenumbers of the selected structures, scaling the relevant modes in y and t, as well as scaling their energy. In principle, the inner region is to be scaled in inner units and the outer region in outer units. However, it is known, for instance from Eitel-Amor *et al.* (2014), that the growth of the structures in the inner region of a TBL is almost negligible compared with the growth of the outer region as we go to higher Re. Moreover, the quickly evolving near-wall structures would compensate for these small differences quite rapidly, as opposed to the slow outer structures. For instance, when comparing $Re_\theta = 2240$ with $Re_\theta = 8000$, the viscous length scale l^* increases by a factor of 1.16, whereas the boundary layer thickness δ_{99} increases by a factor of 3.96. Owing to this, in this work, the inner region from the base Re^{bs} is kept as such, and only the outer region is scaled in outer units in our scaling procedure to reach the target Re^{tg}.

https://doi.org/10.1017/jfm.2026.11689 Published online by Cambridge University Press

For the selected range of k_z^{outer} scaling is performed using the scaling factor, $S_{\delta_{99}}$, computed as

$$S_{\delta_{99}} = \frac{{\delta_{99}}^{tg}}{{\delta_{99}}^{bs}}. \tag{2.6}$$

This scaling factor is 1.9 for the case where velocity slices at $Re_\theta = 4430$ are up-scaled to $Re_\theta = 8000$, and 3.9 when $Re_\theta = 2240$ are scaled up to $Re_\theta = 8000$.

2.2.1. *Scaling in z*

Scaling in the spanwise direction z is performed by means of shifting each of the n retained POD modes of the selected spanwise wavenumbers corresponding to the outer region, k_z^{outer}, to the new position in spectral space. In this work, the first 40 POD modes are kept for all $k_z \in k_z^{outer}$. This preserves approximately 97 % of the turbulent kinetic energy (TKE) across the retained modes. Based on our previous work (Stanly *et al.* 2024), this amount of TKE reduction had no noticeable negative effects on the inflow. Scaling in z is performed as follows and is illustrated with an example in figure 3(*a*):

$$\hat{\varphi_i}^{\left(round\left(k_z/S_{\delta_{99}}\right),n\right)}(y) = \hat{\varphi_i}^{(k_z,n)}(y). \tag{2.7}$$

From here, we use k_z^{outer} to refer to the newly scaled/shifted range of outer k_z, i.e. $k_z^{outer} \approx round(k_z^{outer}/S_{\delta_{99}})$.

2.2.2. *Reconstruction of POD modes to physical space*

Before applying further scaling operations, each POD mode can be independently reconstructed in physical space by applying an inverse Fourier transform to each wavenumber $k_z \in (k_z^{inner} \cup k_z^{outer})$, i.e.

$$\varphi_i^{(k_z,n)}\left(y, z_j\right) = \frac{2}{\sqrt{n_z/2}}\hat{\varphi}_i^{(k_z,n)}(y)e^{2\pi i k_z j/n_z}, \tag{2.8}$$

where the factor 2, within and outside the square root, comes in as we retain only one half of the wavenumbers that exhibit Hermitian symmetry. The factor 2 outside the square root can be removed if $k_z \in (0, (n_z/2))$ as they have no complex conjugate pairs.

2.2.3. *Scaling in y*

Following this, each of the selected POD modes are to be scaled in the wall-normal direction y, as the new structures would grow in y as well, when appearing at the higher Re. To achieve this, while keeping the POD modes the same, the y axis is upscaled such that

$$y^{tg} = y^{bs} \cdot S_{\delta_{99}}. \tag{2.9}$$

If one would now plot the POD modes using this new y^{tg} axis, the modes will look grown in the wall-normal coordinate. However, we need these grown modes on the same initial grid (i.e. y^{bs}). To get this, the next step is to chop off the y^{tg} values beyond $\max(y^{bs})$ such that both meshes go up to the same height. This would result in $\text{size}(y^{tg}) < \text{size}(y^{bs})$, in other words y^{tg} ends up being coarser than y^{bs}. To get back the scaled POD modes to the initial y^{bs}, a two-dimensional spline interpolation is now performed

$$\varphi_i{}^{(k_z,n)}\left(y^{tg}, z\right) \rightarrow \varphi_i{}^{(k_z,n)}\left(y^{bs}, z\right). \tag{2.10}$$

https://doi.org/10.1017/jfm.2026.11689 Published online by Cambridge University Press

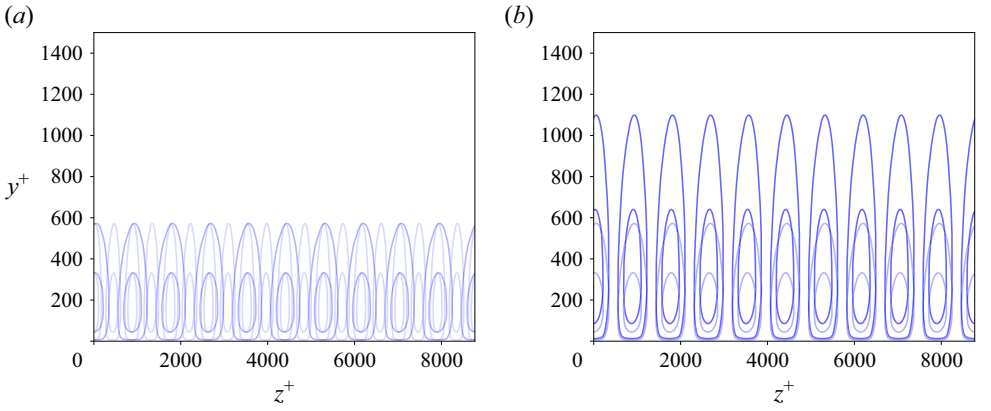


Figure 3. Effect of scaling in k_z and y, illustrated using the real part of the zeroth POD mode at $k_z = 10$ for the streamwise velocity component of *re4k_sc*, i.e. Real$\{\varphi_1^{(k_z=10,n=0)}\}$. In both (*a*) and (*b*), the lighter shade of blue shows the state before scaling, and the darker shade shows the state after scaling. For both, contour lines are plotted for levels [±0.0015, ±0.0030, ±0.0045]. (*a*) Scaling in z, (*b*) scaling in y.

This scaling in y is demonstrated in figure 3(*b*). Since the modes are mapped back to the initial grid (y^{bs}) after scaling, the superscript is partially omitted in further discussions and just y is used.

2.2.4. *Scaling in t*

Next, the time coefficients have to be adjusted as the newly produced bigger structures in the outer region are expected to convect slower than the initial smaller counterparts. Thus, the time array is downscaled by $S_{\delta_{99}}$. Subsequently, the new set of time coefficients are produced by interpolating the old ones on the new time axis. This can be shown as

$$t^{tg} = t^{bs}/S_{\delta_{99}}, \tag{2.11}$$

and for the coefficients

$$a^{(k_z,n)}\left(t^{bs}\right) \rightarrow a^{(k_z,n)}\left(t^{tg}\right). \tag{2.12}$$

2.2.5. *Scaling the energy*

For upscaling the energy of the outer structures, the square of the scaling factor ($S_E{}^2$) is computed between the mean streamwise turbulence intensity ($u'u'$) from the log and outer regions (say, $y^+ > 100$) of the base *Re* obtained from the database, and the mean streamwise turbulence intensity at the target *Re* in the same region (i.e. $y^+ > 100$). For the latter, the following expression proposed by Alfredsson, Segalini & Örlü (2011) is used:

$$\frac{u^{tg}_{rms}\left(y^{bs}\right)}{U_1^{tg}\left(y^{bs}\right)} = 0.031 + 0.260\left(1 - \frac{U_1^{tg}\left(y^{bs}\right)}{U_\infty}\right). \tag{2.13}$$

Although this scaling factor for energy corresponds to the streamwise fluctuations alone, due to lack of other estimates to find scaling factors for fluctuations in the wall-normal and spanwise directions (and following some tests) the same factor is applied to upscale the energy of the wall-normal and spanwise fluctuations as well. This is done by multiplying this energy scaling factor to the corresponding outer modes of the three velocity components in the reconstruction phase. This scaling factor for energy is found to be $S_E \approx 1.3$ for the case where velocity slices at $Re_\theta = 4430$ are up-scaled to $Re_\theta = 8000$,

https://doi.org/10.1017/jfm.2026.11689 Published online by Cambridge University Press

and $S_E \approx 1.5$ when $Re_\theta = 2240$ is scaled up to $Re_\theta = 8000$. This factor, S_E, for energy is applied in the reconstruction phase that follows. Note that a POD mode needs to be scaled with the same factor in order to maintain mass conservation of the disturbances. This property is essential for high-fidelity inflow conditions, as e.g. discussed in Stanly *et al.* (2026).

2.3. *Reconstruction*

The generated mean velocity profiles, $U_i^{tg}(y)$, the selected inner modes and the scaled outer modes are used to reconstruct the velocity fields, $u_i^{tg}(y, z, t^{tg})$, at the target Reynolds number. Note that the scaling of energy of the outer modes using the scaling factor S_E is performed at this stage. The reconstruction is mathematically formulated as follows:

$$\begin{aligned} u_i^{tg}\left(y^{bs}, z, t^{tg}\right) = U_i^{tg}\left(y^{bs}, z\right) \quad (\text{for } k_z = 0,\ n = 0) \\ + \sum_{k_z \in k_z^{inner}} \sum_{n=0}^{n_{modes}-1} a^{(k_z,n)}\left(t^{tg}\right) \varphi_i^{(k_z,n)}\left(y^{bs}, z\right) \\ + \sum_{k_z \in k_z^{outer}} \sum_{n=0}^{n_{modes}-1} S_E \cdot a^{(k_z,n)}\left(t^{tg}\right) \varphi_i^{(k_z,n)}\left(y^{bs}, z\right). \end{aligned} \tag{2.14}$$

This entire process is outlined in Algorithm 1, where $\mathcal{F}_z$ and $\mathcal{F}_z^{-1}$ represent implementations of the fast Fourier transforms, such as the Matlab operations `fft()` and `ifft()`, i.e. the forward and inverse transform, respectively. The normalisations performed on them (i.e. on the output from these functions), in steps 1 and 11 using the factor $\sqrt{n_z/2}$, yield (2.1) and (2.8) after accounting for the normalisation within these Matlab functions.

3. Results

The proposed method is evaluated in two ways:

(i) Assessing the quality of the generated two-dimensional velocity slices that will be used as an inlet condition in § 3.1.
(ii) Applying those velocity planes as an inflow condition and analysing the evolution of a TBL starting at $Re_\theta = 8000$ in § 3.2.

To that end, time-dependent velocity slices at $Re_\theta = 2240$ and $Re_\theta = 4430$ from an available database (Eitel-Amor *et al.* 2014) are scaled up to $Re_\theta^{tg} = 8000$ using the proposed method and compared against the data at $Re_\theta = 8000$ available from the database.

These first two sets of scaled velocity planes will now be referred to as *re2k_sc* and *re4k_sc*, indicating the used Re^{bs}, and *_sc* showing that the data are scaled. The reference planes at $Re_\theta = 8000$ will be referred to as *re8k*. Note that all three datasets are in principle at $Re_\theta^{tg} = 8000$. The TBL simulated using the *re8k* inflow data is essentially the classic precursor-based simulation.

By construction, the scaled velocity planes (*re2k_sc* and *re4k_sc*) have a gap in the pre-multiplied spectra (see figure 4*a*), which needs to be filled up during adaptation. To examine if the scaled cases fill up this missing region in a reasonable way, we add an extra case for comparison. In particular, we modify the reference *re8k* data by removing spanwise wavenumbers approximately in the range $500 < \lambda_z^+ < 1400$, thus introducing the

https://doi.org/10.1017/jfm.2026.11689 Published online by Cambridge University Press

Algorithm 1: Scaling of velocity fields from Re^{bs} to Re^{tg}

Input: $u_i^{bs}(y^{bs}, z, t^{bs}), Re^{tg}$
Derived input: $U_i^{tg}(y^{bs})$, $S_{\delta_{99}}$, S_E, n_{modes}
Output: $u_i^{tg}(y^{bs}, z, t^{tg})$

Perform DFT in z: $\hat{u_i}^{(k_z)}(y^{bs}, t^{bs}) \leftarrow \mathcal{F}_z[u_i^{bs}(y^{bs}, z, t^{bs})]/\sqrt{n_z/2}$
for each $k_z \in [0, n_z - 1]$ **do**
  Compute POD via SVD: $\hat{u_i}^{(k_z)}(y^{bs}, t^{bs}) \approx \sum_{n=0}^{n_{modes}-1} a^{(k_z,n)}(t^{bs})\hat{\varphi_i}^{(k_z,n)}(y^{bs})$
end do
Classify k_z into inner and outer spectral ranges: k_z^{inner}, k_z^{outer}
for each $k_z \in k_z^{outer}$ **do**
  Scale in z:
    $\hat{\varphi_i}^{(round(k_z/S_{\delta_{99}}),n)}(y^{bs}) \leftarrow \hat{\varphi_i}^{(k_z,n)}(y^{bs})$
end do
From here, k_z^{outer} corresponds to the new scaled range of outer k_z, *i.e.,* $k_z^{outer} \approx \text{round}(k_z^{outer}/S_{\delta_{99}})$
Inverse DFT of each POD mode for all $k_z \in (k_z^{inner} \cup\ k_z^{outer})$: $\varphi_i^{(k_z,n)}(y^{bs}, z) \leftarrow \mathcal{F}_z^{-1}[\hat{\varphi_i}^{(k_z,n)}(y^{bs})] \cdot \sqrt{n_z/2}$
for each $k_z \in k_z^{outer}$ **do**
  Scale in y:
    Upscale y-axis: $y^{tg} \leftarrow y^{bs} \cdot S_{\delta_{99}}$
    Remove $y^{tg} > \max(y^{bs})$ such that $\max(y^{tg}) \approx \max(y^{bs})$. Consequently, $\text{size}(y^{tg}) < \text{size}(y^{bs})$ (*i.e.,* y^{tg} ends up as a coarser grid than y^{bs})
    2-D interpolate POD modes from the upscaled, coarse $y^{tg}-$grid onto the finer *base* $y^{bs}-$grid: $\varphi_i{}^{(k_z,n)}(y^{tg}, z) \rightarrow \varphi_i{}^{(k_z,n)}(y^{bs}, z)$
  Scale in t:
    $t^{tg} \leftarrow t^{bs}/S_{\delta_{99}}$
    1-D interpolate POD time coefficients onto the scaled time axis : $a^{(k_z,n)}(t^{bs}) \rightarrow a^{(k_z,n)}(t^{tg})$
end do

Reconstruct velocity fields at Re^{tg} :

$$u_i^{tg}(y^{bs}, z, t^{tg}) \leftarrow \quad U_i^{tg}(y^{bs}) \quad (\text{for } k_z = 0,\ n = 0)$$
$$+ \sum_{k_z \in k_z} \sum_{n=0}^{n_{modes}-1} a^{(k_z,n)}(t^{tg})\varphi_i^{(k_z,n)}(y^{bs}, z)$$
$$+ \sum_{k_z \in k_z^{outer}} \sum_{n=0}^{n_{modes}-1} S_E \cdot a^{(k_z,n)}(t^{tg})\varphi_i^{(k_z,n)}(y^{bs}, z)$$

https://doi.org/10.1017/jfm.2026.11689 Published online by Cambridge University Press

Dataset	Description
re2k_sc	Rescaling $Re_\theta^{bs} = 2240 \rightarrow Re_\theta^{tg} = 8000$ with the proposed method.
re4k_sc	Rescaling $Re_\theta^{bs} = 4430 \rightarrow Re_\theta^{tg} = 8000$ with the proposed method.
re8k	Data at $Re_\theta^{tg} = 8000$ directly from the database (Eitel-Amor *et al.* 2014).
re8k_onlyIO	The *re8k* data but with spanwise wavelengths $500 < \lambda_z^+ < 1400$ removed.

Table 1. Inflow datasets generated for the performance evaluation of the proposed method.

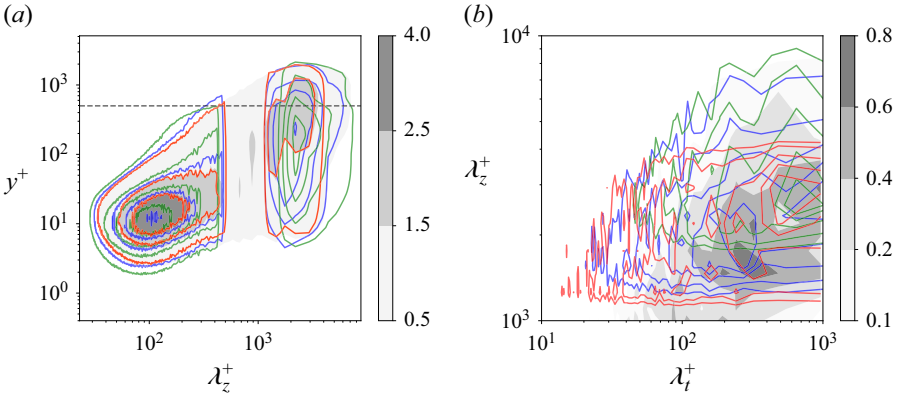


Figure 4. (*a*) One-dimensional pre-multiplied spectra of streamwise velocity u, i.e. $E_{uu}^+(k_z) \cdot k_z$, and (*b*) two-dimensional pre-multiplied power spectral density (PSD) of u in terms of λ_z^+ and λ_t^+, i.e. $E_{uu}^+(k_t k_z) \cdot k_t k_z$, at $y \approx 0.2\delta_{99_0}$ (this height is marked using a dashed horizontal line in (*a*)). In both figures, the reference data *re8k* are shown in the background as filled contours using shades of grey with levels as shown in the colour bar. The *re2k_sc*, *re4k_sc* and *re8k_onlyIO* data are shown using green, blue and red contour lines, respectively, with the contour levels matching those used for the *re8k* data.

same gap as in the scaled data. This additional set of planes is referred to as *re8k_onlyIO*, which stands for 'only inner and outer' regions. A summary of all four generated inflow datasets can be found in table 1.

3.1. *Quality of the inflow velocity slices*

The newly generated time-dependent, two-dimensional velocity slices of the cases *re2k_sc* and *re4k_sc* at the target $Re_\theta^{tg} = 8000$ are assessed here in comparison with the reference *re8k* and *re8k_onlyIO* data, before applying them as an inflow condition in § 3.2.

Figure 4(*a*) shows one-dimensional pre-multiplied spectra of streamwise velocity of the different cases. The gap in the spectra of the scaled cases (i.e. *re2k_sc* and *re4k_sc*), which arises due to the scaling procedure in k_z (as described in § 2.2.1), as well as the intentional gap in *re8k_onlyIO*, are visible in the approximate range of $500 < \lambda_z^+ < 1400$. Outside the gaps, the spectra are well represented. In order to examine if the temporal evolution of the scaled outer structures are reproduced in an acceptable manner, two-dimensional pre-multiplied spectra (in span and time) are computed at a height $y \approx 0.2\delta_{99}^{tg}$, as shown in figure 4(*b*). Despite the apparent noise due to the limited time series, all cases reproduce the strong outer peak in a similar position in the spectra.

In order to examine the effect of energy scaling, we look at the Reynolds stress profiles in figure 5. Due to the fact that the precursor database had time series data sampled on

https://doi.org/10.1017/jfm.2026.11689 Published online by Cambridge University Press

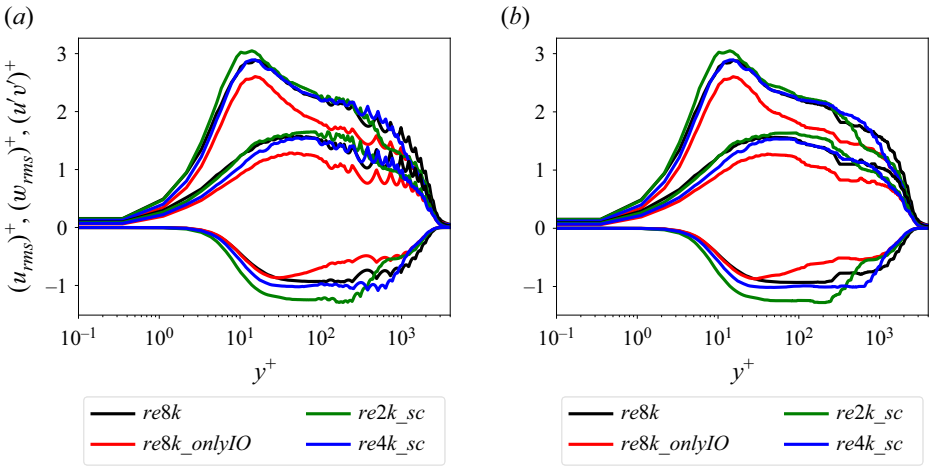


Figure 5. Reynolds stress profiles of the inlet velocity slices. Plot (*a*) shows the raw data whereas the data in (*b*) are obtained by applying a median filter to the raw data to facilitate visual inspection. The wiggles in the raw values are due to the coarse wall-normal resolution in the precursor data.

a coarse y-grid of approximately 47 points, these profiles are wiggly in the outer region. Nevertheless, that does not affect the proposed method.

Owing to the way in which the scaling of energy is performed (see § 2.2.5), the scaled profiles may exhibit a slight over-prediction of energy throughout the profile and not just away from the wall. Specifically, this is due to the wall-attached nature of the large structures that are scaled. This explains why the scaled cases have higher energy than the *re8k_onlyIO* case, which has similar spanwise structures missing, but has the right amount of fluctuations in the structures that are retained.

The difference in energy content between the *re8k* reference case and the *re8k_onlyIO* case is caused entirely by the missing spanwise wavenumbers in the pre-multiplied spectra. Looking at the region (i.e. approximately $100 < y^+ < 2000$) where the scaling of energy is applied, one sees how the u_{rms} and w_{rms} profiles of the scaled cases lift up from the $re8k_onlyIO$ curve and overlap the *re8k* curve – showing that scaled outer structures are slightly over-stimulated to account for the energy of the missing structures. The Reynolds shear-stress curve shows that the scaled cases slightly over-shoot the *re8k* case, which potentially stems from the fact that the scaling factor in v_{rms} may not be exactly the same as that of u_{rms}.

3.2. *Application as inflow condition*

3.2.1. *Computational set-up*

The robustness and accuracy of the proposed method is now examined by using the velocity slices as a Dirichlet inlet condition in the computational fluid dynamics solver Neko (Jansson *et al.* 2024). Neko is a continuous Galerkin spectral element code for the incompressible Navier–Stokes equations. Velocity–pressure decoupling is performed using the $P_N - P_N$ formulation, time integration is third-order semi-implicit and dealiasing of the convective term is performed using the 3/2-rule (Deville, Fischer & Mund 2002; Rezaeiravesh *et al.* 2021). A flat plate at $Re_\theta = 8000$ is set up on a domain with 6.3×10^6 hexahedral elements using seventh-order Gauss–Lobatto–Legendre polynomials, resulting in a total of 3.2×10^9 grid points with spacing as shown in table 2. In the wall-normal region denoted as Y_1, tanh spacing with a growth factor of 2.5 is used; whereas in the Y_2 region, geometric stretching with a stretching parameter of 1.18 is used.

https://doi.org/10.1017/jfm.2026.11689 Published online by Cambridge University Press

Length	Grid points (Ele × GLL)	GLL spacing (in inner units)	Element size (in θ_0)
$L_x = 100\,\theta_0$	$400 \times 8 = 3200$	$\Delta x^+ = 4.7 - 15.5$ Avg = 10.13	0.25
$Y_1 = 0 - 16\,\theta_0\ (0 - 2\,\delta_{99_0})$	$60 \times 8 = 480$	$\Delta y^+ = 0.3 - 41$ Avg = 20	$0.02 - 0.6$ Avg = 0.3
$Y_2 = 16 - 40\,\theta_0\ (2 - 5\,\delta_{99_0})$	$10 \times 8 = 80$	$\Delta y^+ \approx 19 - 277$ Avg = 148	$1.0 - 4.5$ Avg = 2.7
$L_z = 29.6\,\theta_0$	$225 \times 8 = 1800$	$\Delta z^+ = 2.5 - 8.0$ Avg = 5.3	0.13
Total points:(Ele × GLL)	$(6.3 \times 10^6) \times 8^3 = 3.2 \times 10^9$		

Table 2. Details of the Neko direct numerical simulation (DNS) grid used for TBL simulations. The two regions Y_1 and Y_2 split the total domain size in the wall-normal direction, L_y. 'Ele' stands for the number of spectral elements used for spatial discretisation, 'GLL' stands for the number of Gauss–Lobatto–Legendre points used within each element and 'Avg' stands for average.

The average grid spacing in the outer region is approximately 15 Δy^+ at the inlet and approximately 20 Δy^+ at the outlet.

In what follows, we use the subscript 0 to refer to the value of a quantity at the inlet, for example, $\theta_0 = \theta(x)\,|_{x=0}$. The inflow velocity slices are spaced in time approximately $0.044\,\theta_0/U_\infty$ (or $0.47\,l_0^*/u_{\tau_0}$) apart, which fits approximately 20 time steps in Neko. A third-order Lagrange interpolation is performed to obtain inflow fields in between. The database contains a total of 19,410 time instances, which corresponds to approximately $3.7\,\delta_{99_0}/u_{\tau_0}$. From the flat plate TBL simulations, the first $0.88\,\delta_{99_0}/u_{\tau_0}$ (2 flow through times) is removed to account for initial transients, and time and span averaging is performed for the next $2.8\,\delta_{99_0}/u_{\tau_0}$ (≈ 6.4 flow through times). To ensure temporal convergence, one case was run for 3 more flow through times and no significant change was observed. Turbulent statistics are collected in Neko in a similar way as done by Massaro *et al.* (2024*a*). Some parts of the post-processing were performed using PySEMTools (Perez *et al.* 2025). Time series data are also collected from two cross-stream planes of probes located at two downstream locations ($x = 50\,\theta_0$ and $95\,\theta_0$ corresponding to a location in the middle and towards the end of the domain of total length $L_x = 100\,\theta_0$) for the same duration as that of collection of statistics. In terms of the other boundary conditions, an outflow condition is applied at the streamwise end of the domain, a no-slip condition is applied at the bottom wall and periodicity is enforced in the spanwise direction. At the top boundary, outflow is allowed in the normal direction and a full-slip condition is used for the wall-parallel components of velocity.

3.2.2. *Development of the turbulent boundary layer*

Here, the TBL produced by the proposed method (*re2k_sc* and *re4k_sc*) is evaluated by examining its downstream development in comparison with the classic precursor simulation (*re8k*). Since the proposed method introduces large-scale structures that are absent in the corresponding base case, and since the scaled planes exhibit a gap in the spanwise wavenumbers, two main questions arise. Firstly, whether the newly introduced large-scale structures will fade away or continue to grow downstream, and secondly, whether and how fast can the gap in the spectra be filled in.

To answer these questions, we examine the pre-multiplied spectra of u at $x = 50\,\theta_0$ and $x = 95\,\theta_0$, and compare them with those at the inlet (figure 6). Clearly, the large-scale

https://doi.org/10.1017/jfm.2026.11689 Published online by Cambridge University Press

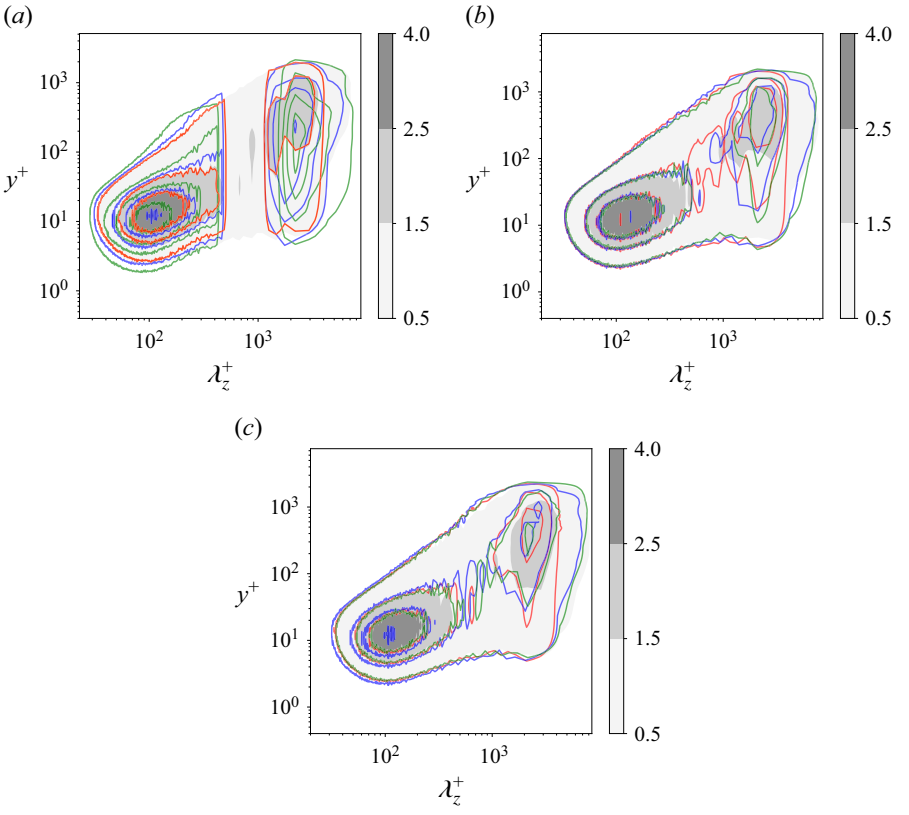


Figure 6. One-dimensional pre-multiplied spectra of streamwise velocity u, i.e. $E_{uu}(k_z) \cdot k_z/u_\tau^2$, at streamwise positions (*a*) $x = 0\,\theta_0$; $Re_\theta \approx 8000$, (*b*) $x = 50\,\theta_0$; $Re_\theta \approx 8500$ and (*c*) $x = 95\,\theta_0$; $Re_\theta \approx 9000$. In all three figures, the reference data *re8k* are shown in the background as filled contours using shades of grey with levels as shown in the colour bar. The *re2k_sc*, *re4k_sc* and *re8k_onlyIO* data are shown using green, blue and red contour lines, respectively. All three show the same contour levels as *re8k*, but without using any shades of the respective colour. Here, the superscript $^+$ indicates normalisation using inner units at the respective *Re*.

structures survive throughout the domain. Furthermore, the wavenumber gap gets filled up quickly within a few integral boundary layer thicknesses δ_{99}. The main production mechanism close to the wall (the inner peak) is already well established at the inlet, so that only the transport along the overlap ridge needs to be initiated. Interestingly, the scaled cases fill up faster and match the reference *re8k* case better than the *re8k_onlyIO* simulation. Looking at the largest wavelengths, it is evident that scaling the energy helps matching the shape of the spectra of the large-scale structures of the reference *re8k* case. The slight deviations in the inner region at the inlet, due to not having scaled the inner region, are also gone by the time the flow reaches the middle of the domain.

In order to get a better picture of how the turbulent fluctuations evolve downstream of the inlet, we look at the streamwise evolution of the Reynolds stress profiles in figure 7. There, all the profiles starting from the inlet and up to $Re_\theta \approx 8700$ are shown together. Since the inflow data are coarsely sampled in y (see figure 5), it takes a distance of $12\,\theta_0 \approx 1.4\,\delta_{99_0}$ for the Reynolds stress profiles to become smooth. Thereafter, *re4k_sc* reaches $Re_\theta \approx 8700$ earliest at a downstream location of $x = 61\,\theta_0 \approx 7.3\,\delta_{99_0}$ from the inlet,

https://doi.org/10.1017/jfm.2026.11689 Published online by Cambridge University Press

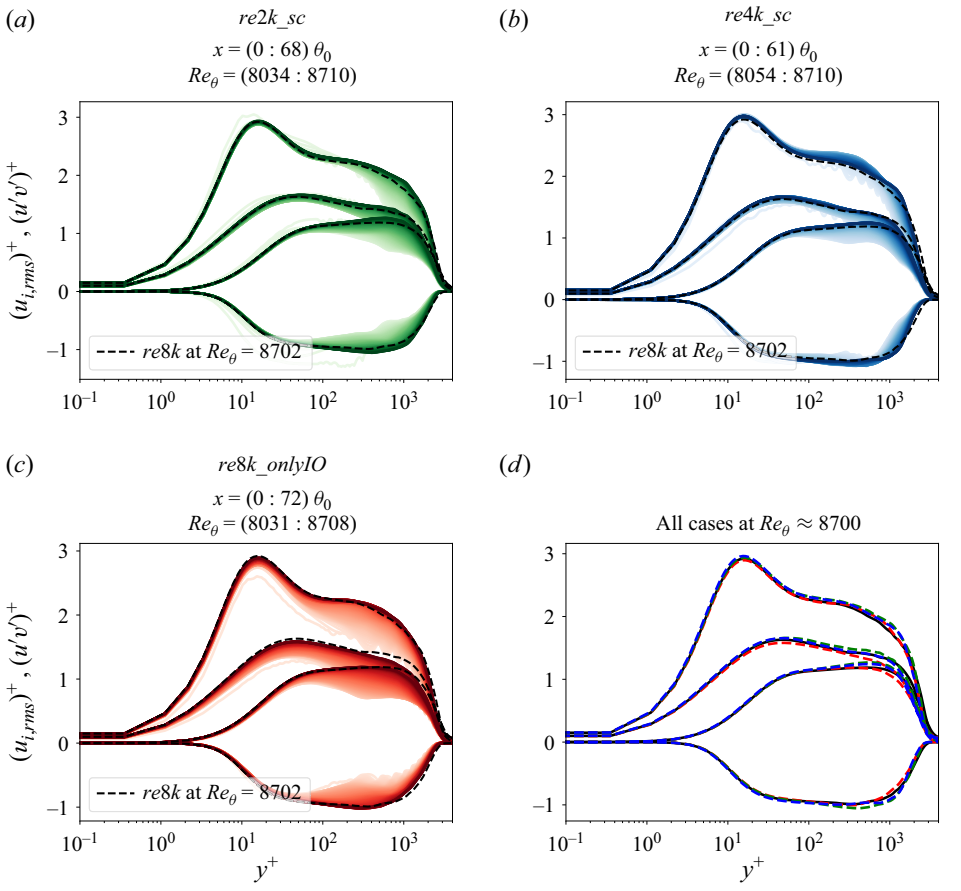


Figure 7. Streamwise development of Reynolds stress profiles for the different cases up to $Re_\theta = 8700$ as compared with *re8k*. Light to darker shades show increasing streamwise distance and $^+$ indicates normalisation using inner units at the inlet.

followed by *re2k_sc* at $x = 68\,\theta_0 \approx 8.1\,\delta_{99_0}$ and lastly *re8k_onlyIO* at $x = 72\,\theta_0 \approx 8.6\,\delta_{99_0}$. At that position, as seen in figure 7(*d*), *re2k_sc* and *re4k_sc* match the profiles of *re8k* much better than that of *re8k_onlyIO*. The latter under-predicts all the Reynolds stresses.

Provided that the two scaled cases resulted in excellent agreement for Reynolds stresses at approximately the same downstream distance of $\approx 8\,\delta_{99_0}$, the performance of the proposed method may be largely Re^{bs}-independent.

In figure 8, the development length is further examined using the usual measures of inner- and outer-scale convergence (Chauhan *et al.* 2009; Schlatter & Örlü 2012): the skin friction coefficient, c_f, and the shape factor, H_{12}, respectively. The development is shown against Re_θ in figure 8(*a*), and against two non-dimensionalised streamwise distances in figure 8(*b*). The latter can be examined together with figure 8(*c*), where Re_θ is plotted against different non-dimensionalised streamwise distances. As a side note, it is worth mentioning that, here, θ and H_{12} are calculated by integrating up to the top of the domain and taking $U_\infty = 1$.

One of those non-dimensional distances shown in figures 8(*b*) and 8(*c*) is x/δ_{99_0}, which is the most common unit of measure for the adaptation length. Another one is based on the large-eddy turn-over length $\delta_{99}U^+_\infty$, following the suggestion by Simens *et al.* (2009) and

https://doi.org/10.1017/jfm.2026.11689 Published online by Cambridge University Press

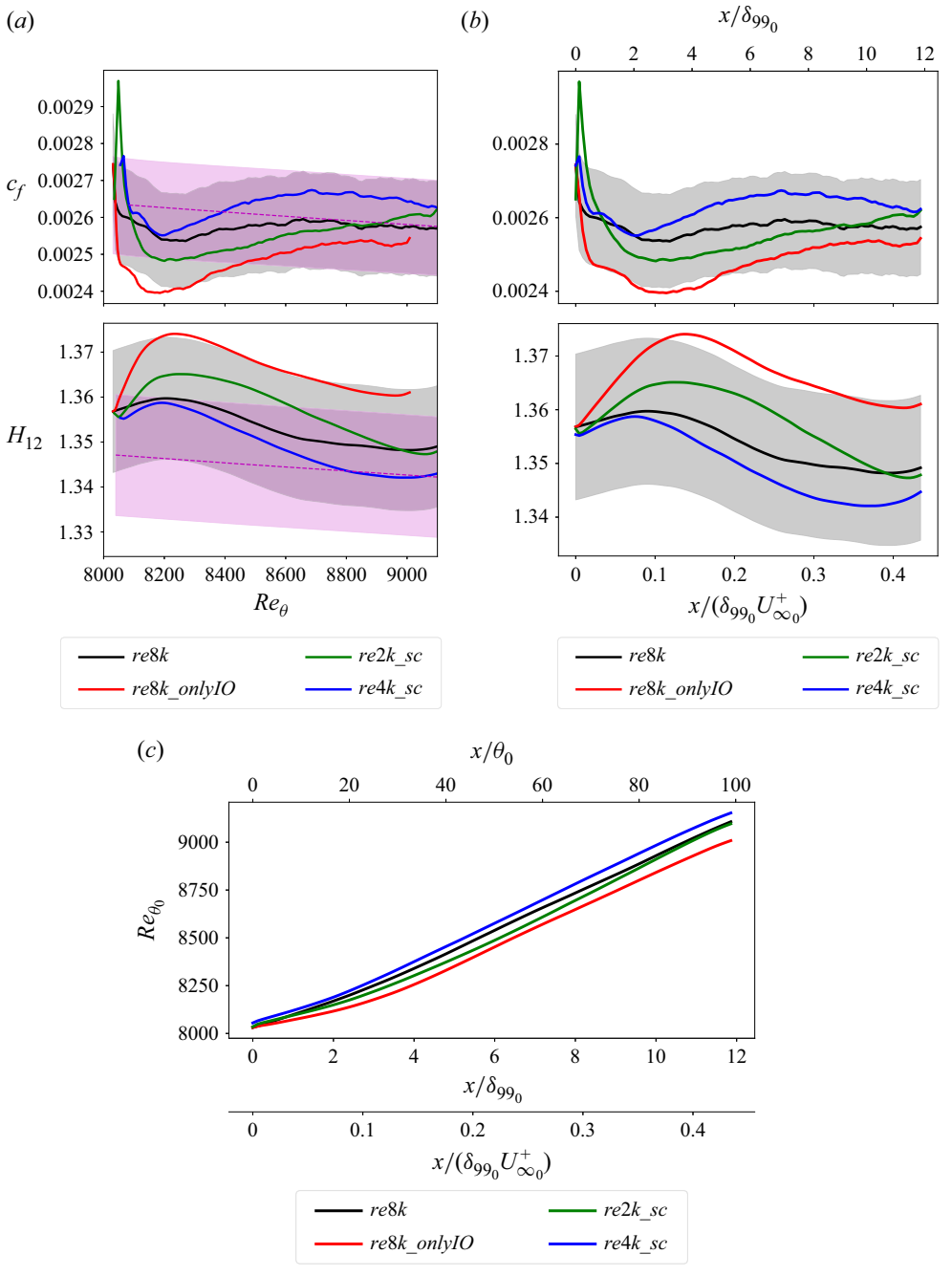


Figure 8. Development of skin friction coefficient, c_f, and shape factor, H_{12} plotted against (*a*) Re_θ and (*b*) non-dimensional streamwise distance. In (*a*), the dashed line in magenta is the Coles–Fernholz relation and correlation, both by Chauhan, Monkewitz & Nagib (2009), for c_f and H_{12}, respectively. The shaded magenta regions show the ± 5 % and ± 1 % tolerances with respect to the corresponding dashed magenta lines. In both (*a*) and (*b*), the grey-shaded region depicts the same tolerance but with respect to *re8k*. (*c*) Development of Re_θ against different non-dimensionalised streamwise distances. The maximum spread in Re_θ at the inlet is 0.3 % and that at the outlet is 1 %, both with respect to *re8k*.

https://doi.org/10.1017/jfm.2026.11689 Published online by Cambridge University Press

used by Sillero *et al.* (2013). It characterises the development length based on how far the eddies advect in a large-eddy turnover time δ_{99}/u_τ (Sillero *et al.* 2013). Although here we use $\delta_{99_0}U^+_{\infty_0}$ instead, it is expected to be reasonably similar to $\delta_{99}U^+_\infty$ owing to the short length of the domain. For example, δ_{99} grows only by a factor 1.13 from the inlet to the outlet.

We begin by discussing the development of c_f in comparison with the Coles–Fernholz relation, and H_{12} against a correlation, both by Chauhan *et al.* (2009). There is usually $\pm 5\,\%$ and $\pm 1\,\%$ spread between DNS and experimentally measured c_f and H_{12}, respectively, with respect to these correlations even for high-quality data (Örlü & Schlatter 2013; Sillero *et al.* 2013; Eitel-Amor *et al.* 2014), and such tolerances are shown in figure 8(*a*). The c_f values of both the scaled cases, *re2k_sc* and *re4k_sc*, as well as that of the precursor reference simulation, *re8k*, stay within the $\pm 5\,\%$ margin with respect to the correlations right from the inlet. It is only the *re8k_onlyIO* case that briefly drifts outside this tolerance shortly after the inlet. In terms of H_{12}, both the reference *re8k* and the scaled *re4k_sc* case stay within these acceptable margins with respect to the correlations throughout the domain straight away from the inlet. The H_{12} curve of *re2k_sc* comes into this region at $Re_\theta \approx 8600$ ($\approx 7.5\,\delta_{99_0}$ or $\approx 0.28\,\delta_{99_0}U^+_{\infty_0}$). On the other hand, the *re8k_onlyIO* case always stays outside these margins throughout the domain.

The development length of the *re8k* case is visible up to $Re_\theta \approx 8600$, (i.e. $\approx 6.5\,\delta_{99_0}$ or $\approx 0.26\,\delta_{99_0}U^+_{\infty_0}$) and is caused by the coarse $y-$spacing of the inlet data and the time interpolation performed between two subsequent inlet velocity planes. As such these sources of errors are present in all cases we study here and are unrelated to the proposed inflow method. This necessitates a comparison with similar margins with respect to the *re8k* case. All cases, including *re8k_onlyIO*, always stay within the $\pm 5\,\%$ and $\pm 1\,\%$ deviations from *re8k*, for c_f and H_{12}, respectively. In fact, the scaled cases are always within $\pm 3.5\,\%$ and $\pm 0.5\,\%$ with respect to *re8k* for these two quantities, right from the inlet, which is uncommon with inflow methods that are not precursors.

Considering all the above-mentioned observations for the scaled cases, including the developments of Reynolds stresses in figure 7, and c_f and H_{12} in figure 8, we conclude that the new scaling procedure-based inflow generation method results in a development length largely determined by the development of Reynolds stresses. This development length is approximately $8\,\delta_{99_0}$ or $0.3\,\delta_{99_0}U^+_{\infty_0}$, for the cases studied here. This is at least one order of magnitude shorter than other high Re inflow studies in the literature. Notably, in the work by Sillero *et al.* (2013), where they performed DNS of a TBL up to $Re_\theta = 6000$ and where the development length was dominated by the adaptation of large-scale structures, a development length of $3-4\,\delta_{99}U^+_\infty$ was needed for H_{12} to reach within $\approx \pm 1\,\%$ tolerance of an empirical fit. And based on Simens *et al.* (2009), the relaxation of most flow scales needs at least $1\,\delta_{99}U^+_\infty$, which is not true for the current method. We avoid having to wait for the adaptation of the time-consuming large-scale structures by introducing their physically accurate description, as well as retaining the near-wall structures. The short development length is determined by how the region in the middle of the inner and outer regions in the spanwise pre-multiplied spectra is filled. This can be monitored indirectly by following the streamwise development of the Reynolds stress profiles.

4. Conclusions and outlook

We presented an inflow generation method based on up-scaling a set of two-dimensional precursor velocity slices in spectral space from a lower base Re to higher target Re to be used as inflow condition for spatially developing TBLs. Apart from the precursor data at

https://doi.org/10.1017/jfm.2026.11689 Published online by Cambridge University Press

the lower base Re (which could be taken from an existing database, if the width matches the $target$ domain, such as the one we use here), this method only needs the value of the target Re as input.

The essence of the method involves providing a rich description of the computationally expensive large-scale structures as well as the physically relevant near-wall structures. This helps it to evade the usual factor that results in large development lengths for high Re TBLs – the development of slow evolving outer structures. As such, the proposed method resulted in a development length ($\approx 8\,\delta_{99_0}$) that is one order of magnitude shorter than other high Re TBL DNS in the literature. Since the usual measures, such as the development of c_f and H_{12}, gave reasonable agreement with the reference precursor simulation right from the inlet, the development length of the proposed method is determined by how the missing fluctuations in the pre-multiplied spectra got filled up and is tracked using the streamwise evolution of the Reynolds stress profiles.

The method worked seamlessly when base $Re_\theta = 2240$ and 4430 were used to produce target $Re_\theta = 8000$. Starting from precursor data at a base Re high enough, such that outer scaling holds true, is necessary to seamlessly obtain the correct pre-multiplied spectra at the target Re using the scaling procedure. Nevertheless, in the interest of further stress testing the method, we ran it using data from a very low base $Re_\theta = 790$. Scaling this, on the other hand, required a couple of iterations of trial and error to find the right scaling parameters for space and energy to correctly match the pre-multiplied spectra at the target Re. If one has access to such spectra at the target Re, for instance from experimental measurements or obtained by applying the scaling procedure to one of the base Re used in this work, then such a trial and error exercise is worthwhile in the interest of going further down in the precursor base Re. Going to lower base Re could be helpful if the existing database cannot be used. For instance, if the width of the target domain does not match with that of the database, which necessitates a new precursor to be run on a wider domain but at a lower base Re such that it is computationally affordable.

When scaling the base Re velocity slices to target Re, the spanwise width of the base velocity field should be wide enough such that it can fit a couple of the widest structures resulting after scaling to the higher target Re. In order for this to not be a limiting factor for using the proposed method, the best way is to make sure to have a wide enough domain for the base velocity fields. Work arounds to artificially increase the spanwise width of existing data should be done carefully, if not avoided. This can, for instance, be done either using zero padding or by performing a windowing operation before replicating in span, to avoid discontinuities. Directly replicating the data in span, taking advantage of the spanwise periodicity, would result in spectral artefacts like artificial discontinuities due to spectral leakage.

It is necessary to have a long time series of velocity planes, long enough to study the statistics of the evolving TBL without introducing artificial periodicity by restarting from the same set of planes to continue the time signal. One can avoid this by either running a very long precursor at the base Re, or using methods like the vector autoregression based time series extension method recently proposed by Stanly *et al.* (2024). Using this, one can first extend the base Re data to arbitrary lengths in time, and then input them (either as just time coefficients or as reconstructed velocity fields) into the proposed method to scale those to a higher *target Re*.

Although not exploited to its full potential in this work, the SVD performed in the wall-normal direction permits low-order modelling of the wall-normal dynamics. We kept the same n_{modes} across all k_z such that a minimum amount of TKE across all k_z was maintained. It is possible to obtain an optimised n_{modes} for each k_z to enable further reduction in the order of the model while maintaining a required amount of TKE.

https://doi.org/10.1017/jfm.2026.11689 Published online by Cambridge University Press

This is possible as the contribution of different k_z to TKE is different, thereby enabling further truncation.

The proposed method can naturally be applied to other wall-bounded flows, like pipes and channels for instance, to provide efficient inflow conditions at higher Reynolds numbers with minimal initial transients. This method can also be used to provide inflow conditions for high *Re* TBLs in applications such as wind turbine farms, where an atmospheric boundary layer needs to be simulated. Applications to other flows, such as jets and mixing layers, may also be considered, as long as an approximate scaling law of both mean and fluctuating profiles is available.

Acknowledgements. The authors gratefully acknowledge Geert Brethouwer and Shiyu Du for valuable discussions and constructive comments on the manuscript, and Ardeshir Hanifi for insightful discussions. The computations and data handling were enabled by resources provided by the National Academic Infrastructure for Supercomputing in Sweden (NAISS), partially funded by the Swedish Research Council through grant agreement no. 2022-06725. In addition, NAISS is acknowledged for awarding a project access to the LUMI supercomputer, owned by the EuroHPC Joint Undertaking and hosted by CSC (Finland) and the LUMI consortium.

Funding. This project has received funding from the European High-Performance Computing Joint Undertaking (JU) under grant agreement No 101092621. The JU receives support from the European Union's Horizon Europe research and innovation programme and Germany, Italy, Slovenia, Spain, Sweden and France.

Declaration of interests. The authors report no conflicts of interest.

References

Alfredsson, P.H., Segalini, A. & Örlü, R. 2011 A new scaling for the streamwise turbulence intensity in wall-bounded turbulent flows and what it tells us about the "outer'' peak. *Phys. Fluids* **23** (4), 041702.

Biau, D. 2023 Self-similar temporal turbulent boundary layer flow. *Comput. Fluids* **254**, 105795.

Bounchaleun, A. 2019 *An Elementary Introduction to Fast Fourier Transform Algorithms*. University of Chicago REU Paper.

Chauhan, K.A., Monkewitz, P.A. & Nagib, H.M. 2009 Criteria for assessing experiments in zero pressure gradient boundary layers. *Fluid Dyn. Res.* **41** (2), 021404.

Coles, D. 1956 The law of the wake in the turbulent boundary layer. *J. Fluid Mech.* **1** (2), 191–226.

Deville, M.O., Fischer, P.F. & Mund, E.H. 2002 *High-Order Methods for Incompressible Fluid Flow*. Cambridge University Press.

Dhamankar, N.S., Blaisdell, G.A. & Lyrintzis, A.S. 2018 Overview of turbulent inflow boundary conditions for large-eddy simulations. *AIAA J.* **56** (4), 1317–1334.

Eitel-Amor, G., Örlü, R. & Schlatter, P. 2014 Simulation and validation of a spatially evolving turbulent boundary layer up to $Re_\theta = 8300$. *Intl J. Heat Fluid Flow* **47**, 57–69.

Hutchins, N. & Marusic, I. 2007 Evidence of very long meandering features in the logarithmic region of turbulent boundary layers. *J. Fluid Mech.* **579**, 1–28.

Jansson, N., Karp, M., Podobas, A., Markidis, S. & Schlatter, P. 2024 Neko: a modern, portable, and scalable framework for high-fidelity computational fluid dynamics. *Comput. Fluids* **275**, 106243.

Jarrin, N., Benhamadouche, S., Laurence, D. & Prosser, R. 2006 A synthetic-eddy-method for generating inflow conditions for large-eddy simulations. *Intl J. Heat Fluid Flow* **27** (4), 585–593.

Marušić, I. & Perry, A.E. 1995 A wall-wake model for the turbulence structure of boundary layers. Part 2. Further experimental support. *J. Fluid Mech.* **298**, 389–407.

Massaro, D., Peplinski, A., Stanly, R., Mirzareza, S., Lupi, V., Mukha, T. & Schlatter, P. 2024*a* A comprehensive framework to enhance numerical simulations in the spectral-element code Nek5000. *Comput. Phys. Commun.* **302**, 109249.

Massaro, D., Yao, J., Rezaeiravesh, S., Hussain, F. & Schlatter, P. 2024*b* Energy-based characterisation of large-scale coherent structures in turbulent pipe flows. *J. Fluid Mech.* **996**, A45.

Monkewitz, P.A., Chauhan, K.A. & Nagib, H.M. 2007 Self-consistent high-Reynolds-number asymptotics for zero-pressure-gradient turbulent boundary layers. *Phys. Fluids* **19** (11), 115101.

Monty, J.P., Hutchins, N., H.C.H., N.G., Marusic, I. & Chong, M.S. 2009 A comparison of turbulent pipe, channel and boundary layer flows. *J. Fluid Mech.* **632**, 431–442.

https://doi.org/10.1017/jfm.2026.11689 Published online by Cambridge University Press

MONTY, J.P., STEWART, J.A., WILLIAMS, R.C. & CHONG, M.S. 2007 Large-scale features in turbulent pipe and channel flows. *J. Fluid Mech.* **589**, 147–156.

ÖRLÜ, R. & SCHLATTER, P. 2013 Comparison of experiments and simulations for zero pressure gradient turbulent boundary layers at moderate Reynolds numbers. *Exp. Fluids* **54** (6), 1547.

PAMIÈS, M., WEISS, P.-É., GARNIER, E., DECK, S. & SAGAUT, P. 2009 Generation of synthetic turbulent inflow data for large eddy simulation of spatially evolving wall-bounded flows. *Phys. Fluids* **21** (4), 045103.

PEREZ, A., TOOSI, S., OLSEN, T.F., MARKIDIS, S. & SCHLATTER, P. 2026 PySEMTools: a library for post-processing hexahedral spectral element data. *J. Open Source Softw.* **11** (120), 8767.

PERRY, A.E. & CHONG, M.S. 1982 On the mechanism of wall turbulence. *J. Fluid Mech.* **119**, 173–217.

PERRY, A.E. & MARUŠIĆ, I. 1995 A wall-wake model for the turbulence structure of boundary layers. Part 1. Extension of the attached eddy hypothesis. *J. Fluid Mech.* **298**, 361–388.

REZAEIRAVESH, S., JANSSON, N., PEPLINSKI, A., VINCENT, J. & SCHLATTER, P. 2021 Nek5000: theory, implementation, optimization. *Tech. Rep.* KTH Royal Institute of Technology. Available at: https://www.mech.kth.se/~pschlatt/Nek5000_2021.pdf.

ROBINSON, S.K. 1991 Coherent motions in the turbulent boundary layer. *Annu. Rev. Fluid Mech.* **23** (1), 601–639.

SANDBERG, R.D. & SANDHAM, N.D. 2008 Direct numerical simulation of turbulent flow past a trailing edge and the associated noise generation. *J. Fluid Mech.* **596**, 353–385.

SANDHAM, N., YAO, Y. & LAWAL, A. 2003 Large-eddy simulation of transonic turbulent flow over a bump. *Intl J. Heat Fluid Flow* **24** (4), 584–595.

SANDHAM, N.D. & SANDBERG, R.D. 2009 Direct numerical simulation of the early development of a turbulent mixing layer downstream of a splitter plate. *J. Turbul.* **10**, N1.

SCHLATTER, P. & ÖRLÜ, R. 2012 Turbulent boundary layers at moderate Reynolds numbers: inflow length and tripping effects. *J. Fluid Mech.* **710**, 5–34.

SILLERO, J.A., JIMÉNEZ, J. & MOSER, R.D. 2013 One-point statistics for turbulent wall-bounded flows at Reynolds numbers up to $\delta^+ = 2000$. *Phys. Fluids* **25** (10), 105102.

SIMENS, M.P., JIMÉNEZ, J., HOYAS, S. & MIZUNO, Y. 2009 A high-resolution code for turbulent boundary layers. *J. Comput. Phys.* **228** (11), 4218–4231.

SMITS, A.J., MCKEON, B.J. & MARUSIC, I. 2011 High–Reynolds number wall turbulence. *Annu. Rev. Fluid Mech.* **43**, 353–375.

SPALART, P.R. 1988 Direct simulation of a turbulent boundary layer up to $R_\theta = 1410$. *J. Fluid Mech.* **187**, 61–98.

STANLY, R., BAGHERI, E., MUKHA, T. & SCHLATTER, P. 2026 Influence of turbulence inflow conditions on aeroacoustics of wall-bounded flows. *Intl J. Heat Fluid Flow* **118**, 110216.

STANLY, R., DU, S., XAVIER, D., PEREZ, A., MUKHA, T., MARKIDIS, S., REZAEIRAVESH, S. & SCHLATTER, P. 2024 Generating synthetic turbulence with vector autoregression of proper orthogonal decomposition time coefficients. *J. Fluid Mech.* **1000**, A83.

SUBBAREDDY, P., PETERSON, D., CANDLER, G. & MARUSIC, I. 2006 A synthetic inflow generation method using the attached eddy hypothesis. In *24th AIAA Applied Aerodynamics Conference*.

SUBRAHMANYAM, M.A., CANTWELL, B.J. & ALONSO, J.J. 2022 A universal velocity profile for turbulent wall flows including adverse pressure gradient boundary layers. *J. Fluid Mech.* **933**, A16.

TABOR, G.R. & BABA-AHMADI, M.H. 2010 Inlet conditions for large eddy simulation: a review. *Comput. Fluids* **39** (4), 553–567.

TOUBER, E. & SANDHAM, N.D. 2009 Large-eddy simulation of low-frequency unsteadiness in a turbulent shock-induced separation bubble. *Theor. Comput. Fluid Dyn.* **23**, 79–107.

TOWNSEND, A.A.R. 1956 *The Structure of Turbulent Shear Flow*. Cambridge University Press.

TOWNSEND, A.A.R. 1976 *The Structure of Turbulent Shear Flow*. Cambridge University Press.

TREFETHEN, L.N. 2000 *Spectral Methods in MATLAB*. Society for Industrial and Applied Mathematics.

VON KÁRMÁN, T. 1930 Mechanische Ähnlichkeit und turbulenz. In *Nachrichten von der Gesellschaft der Wissenschaften Zu Göttingen, Fachgruppe 1 (Mathematik)*, pp. 58–76. Weidmannsche Buchh.

WEI, T., LI, Z. & WANG, Y. 2023 New formulations for the mean wall-normal velocity and Reynolds shear stress in a turbulent boundary layer under zero pressure gradient. *J. Fluid Mech.* **969**, A3.

WU, X. 2017 Inflow turbulence generation methods. *Annu. Rev. Fluid Mech.* **49** (1), 23–49.

WYNN, A., PARVAR, S., O'CONNOR, J., FRANTZ, R.A.S. & LAIZET, S. 2025 Asymptotic scaling laws for periodic turbulent boundary layers and their numerical simulation up to $Re_\theta = 8300$. *J. Fluid Mech.* **1020**, A6.

https://doi.org/10.1017/jfm.2026.11689 Published online by Cambridge University Press